

Exciton-magnon transitions in the frustrated chromium antiferromagnets CuCrO_2 , $\alpha\text{-CaCr}_2\text{O}_4$, CdCr_2O_4 , and ZnCr_2O_4

M. Schmidt,¹ Zhe Wang,¹ Ch. Kant,¹ F. Mayr,¹ S. Toth,²
A.T.M.N. Islam,² B. Lake,^{2,3} V. Tsurkan,^{1,4} A. Loidl,¹ and J. Deisenhofer¹

¹*Experimental Physics V, Center for Electronic Correlations and Magnetism,
University of Augsburg, D-86135 Augsburg, Germany*

²*Helmholtz Zentrum Berlin für Materialien und Energie, D-14109 Berlin, Germany*

³*Institut für Festkörperphysik, Technische Universität Berlin, D-10623 Berlin, Germany*

⁴*Institute of Applied Physics, Academy of Sciences of Moldova, MD-2028 Chisinau, Republic of Moldova*
(Dated: October 16, 2012)

We report on optical transmission spectroscopy of the Cr-based frustrated triangular antiferromagnets CuCrO_2 and $\alpha\text{-CaCr}_2\text{O}_4$, and the spinels CdCr_2O_4 and ZnCr_2O_4 in the near-infrared to visible-light frequency range. Via the exciton-magnon sidebands of the spin-forbidden crystal-field transitions of the Cr^{3+} ions (spin $S = 3/2$), it is possible to optically trace magnon excitations in the system and search the existence of antiferromagnetic spin correlations even far above the magnetic ordering temperature. For example, in CuCrO_2 the temperature dependence of the line width of exciton-magnon transitions can be associated with the density of topologically protected Z_2 vortices, which were proposed to occur in this class of systems. In $\alpha\text{-CaCr}_2\text{O}_4$ we observe magnon sidebands at energies corresponding to low-lying roton-like spin waves. In CdCr_2O_4 magnon sidebands are found to persist across the magnetic ordering transition up to the corresponding Curie-Weiss temperature, indicating that short-range helical spin correlations are present also in the classical spin-liquid regime between the Néel and the Curie-Weiss temperatures. In ZnCr_2O_4 only a weak fine structure related to the magnetic ordering in the system has been observed.

PACS numbers: 75.30.Ds, 71.70.Ch, 78.30.-j, 78.40.-q

I. INTRODUCTION

An archetype of a geometrically frustrated spin arrangement are antiferromagnetically coupled Ising spins residing on the corners of a triangular lattice. In three dimensions the pyrochlore lattice which can be regarded as a network of corner-sharing tetrahedra is one of the most studied structures to explore the realm of frustration phenomena in magnetism.

These geometrically frustrated lattices may provide evidence for exotic ground states such as spin ice, spin liquids, or spin gels. The latter has been described as a topologically ordered state with finite but extended spin correlations and was proposed to be realized in systems with antiferromagnetically coupled Heisenberg spins on a two-dimensional (2D) triangular lattice.¹ In this case the nearest-neighbor bilinear interaction yields a long-range ordered magnetic state at $T = 0$, where neighboring spins order at an angle of 120° to each other.² Moreover, the model exhibits a topologically stable defect described in terms of a Z_2 vortex³.

A well-known class of triangular antiferromagnets is given by systems with chemical formula $A\text{CrO}_2$ with $A = \text{Cu}, \text{Ag}, \text{Pd}, \text{Li}, \text{Na}$. Depending on the stacking sequence these compounds have either delafossite structure (e.g. Cu/PdCrO_2) or an ordered rock salt type structure (e.g. Li/NaCrO_2). These systems have attracted enormous interest because of a large variety of magnetic and electronic phenomena and the occurrence of multiferroicity. For example, CuCrO_2 and AgCrO_2 reportedly exhibit spin-driven ferroelectricity⁴ and the spin correla-

tions in both rocksalt- and delafossite-type $A\text{CrO}_2$ have been associated with the formation of Z_2 vortices^{5–10}.

Optical studies have been reported in the rocksalt-type systems NaCrO_2 and LiCrO_2 ^{11,12}. These systems exhibit exciton-magnon transitions¹³ in the energy region of the spin-forbidden $^4A_{2g} \rightarrow ^2T_{2g}$ crystal-field excitation of the Cr^{3+} ions. Kojima *et al.* proposed that the lifetime of the exciton-magnon lines in triangular lattice antiferromagnets is directly related to the density of Z_2 vortices in the system.¹² In this work we investigated the delafossite-type system CuCrO_2 by optical spectroscopy. CuCrO_2 crystallizes in space group $R\bar{3}m$ ¹⁴ where layers of the magnetic chromium ions ($3d^3$, $S = 3/2$) are separated by one copper and two oxygen layers [see Fig. 1(a) and (d)]. Due to this distance the system is moderately frustrated with a Curie-Weiss-temperature Θ of 190 K and an antiferromagnetic ordering below $T_{N2} = 24.2$ K. The magnetic transition leads to a slight distortion of the CrO_6 octahedra^{15,16} and an incommensurate proper screw magnetic structure.¹⁷ Specific heat measurements showed that there are actually two successive phase transitions at $T_{N1} = 23.6$ K and $T_{N2} = 24.2$ K.¹⁸ At T_{N2} a two-dimensional antiferromagnetic ordering was proposed and only below T_{N1} three-dimensional magnetic ordering and the occurrence of multiferroicity sets in.¹⁹

Moreover, we investigated the triangular-lattice antiferromagnet $\alpha\text{-CaCr}_2\text{O}_4$, which has an orthorhombically distorted delafossite structure (space group $Pmmn$)²⁰, where the Cr^{3+} ions occupy two crystallographically inequivalent positions [see Fig. 1(b) and (e)]. With a Curie-Weiss temperature of -564 K and a Néel temperature of

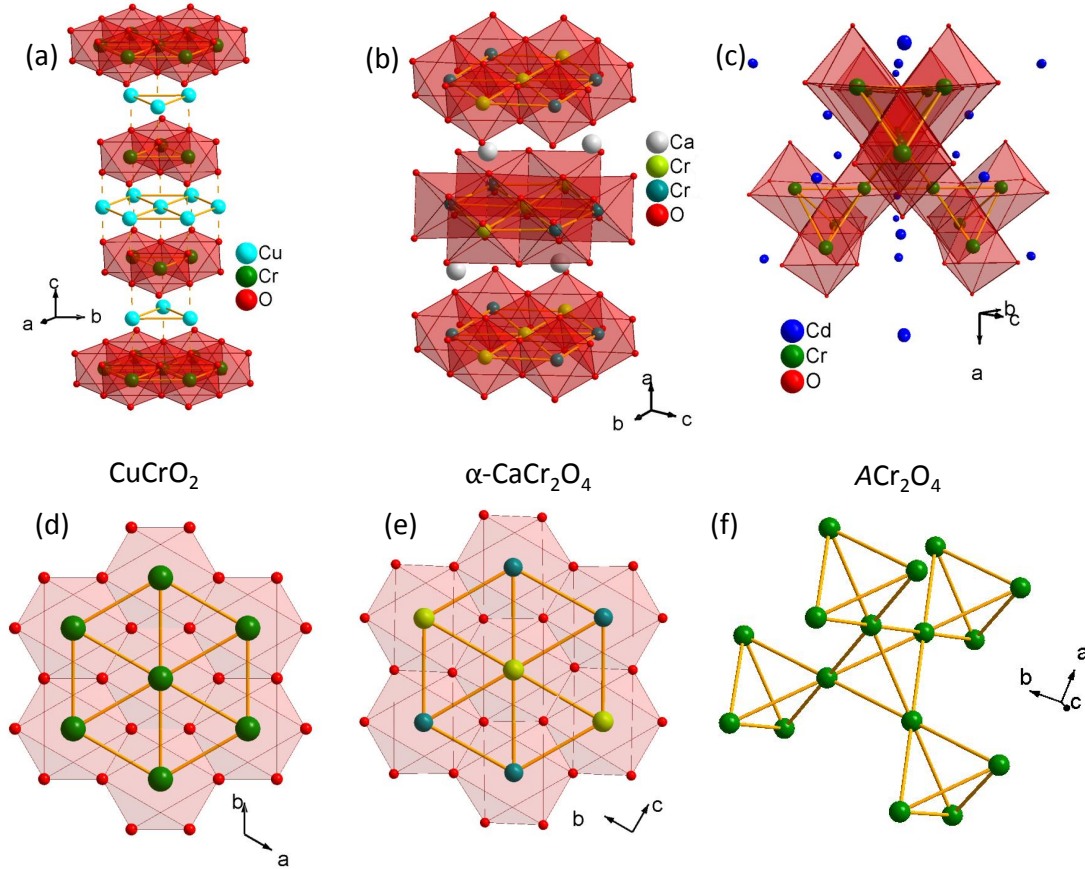


FIG. 1: (Color online) Crystal structures of (a) CuCrO_2 , (b) $\alpha\text{-CaCr}_2\text{O}_4$, and (c) ACr_2O_4 with $A=\text{Cd}, \text{Zn}$. In (d)-(f) we show the respective triangular planes and the pyrochlore lattice for these compounds.

$T_N = 42.6$ K the system is clearly geometrically frustrated and exhibits a planar 120° -spin structure in the crystallographic ac -plane.^{21,22} Recent studies report multiferroicity (also in $\alpha\text{-MCr}_2\text{O}_4$ $M = \text{Sr}, \text{Ba}$)^{23,24} and low-lying magnetic modes with a roton-like dispersion suggesting the presence of competing phases in $\alpha\text{-CaCr}_2\text{O}_4$.²⁵ The related compound $\alpha\text{-SrCr}_2\text{O}_4$ reportedly exhibits similar magnetic properties but is less distorted than $\alpha\text{-CaCr}_2\text{O}_4$.²⁶

The spinel systems CdCr_2O_4 and ZnCr_2O_4 with a pyrochlore lattice of magnetic Cr^{3+} ions [see Fig. 1(c) and (f)] are considered as model systems to study the effects of geometric frustration of Heisenberg spins on the pyrochlore lattice. Further-neighbor exchange interactions²⁷ and magneto-elastic coupling lead to magneto-structural transitions^{28–35} at Néel temperatures of 12.5 K and 7.8 K for ZnCr_2O_4 and CdCr_2O_4 , respectively^{36,37}, while the respective Curie-Weiss temperatures are -390 K and -71 K.^{30,38} The observation of magnetic excitations by neutron scattering which can be modelled by structure factors corresponding to a partition of the pyrochlore lattice into hexagonal loops or even heptamers^{39–41} has contributed considerably to this paradigmatic status. A low-temperature optical absorption spectrum of ZnCr_2O_4 has been reported by Szym-

czak *et al.*⁴², where an exotic multiplet-sideband assigned to exciton-magnon-phonon processes has been observed. A clear suppression of this sideband has recently been reported in ultra-high magnetic fields up to 600 T.⁴³

In this study we will focus on and compare the exciton-magnon transitions related to spin-forbidden CF excitations of the Cr^{3+} ions with spin $S = 3/2$, which are in an octahedral environment in all considered compounds. We assign the magnon sidebands by comparison with available neutron scattering data and discuss their temperature dependence with respect to the structural and magnetic features associated with the effects of geometric spin frustration.

II. EXPERIMENTAL DETAILS AND SAMPLE CHARACTERIZATIONS

Single crystals of CuCrO_2 were prepared by flux-decomposition method using $\text{K}_2\text{Cr}_2\text{O}_7$ flux and CuO . The soaking temperature was 1150°C , the soaking time 20 h and the cooling rate 2°C/h . Plate-like single-crystalline samples with dimension up to $5 \times 5 \times 0.7$ mm³ were prepared. The grown single crystals were checked by x-ray diffraction and no impurity phases could be

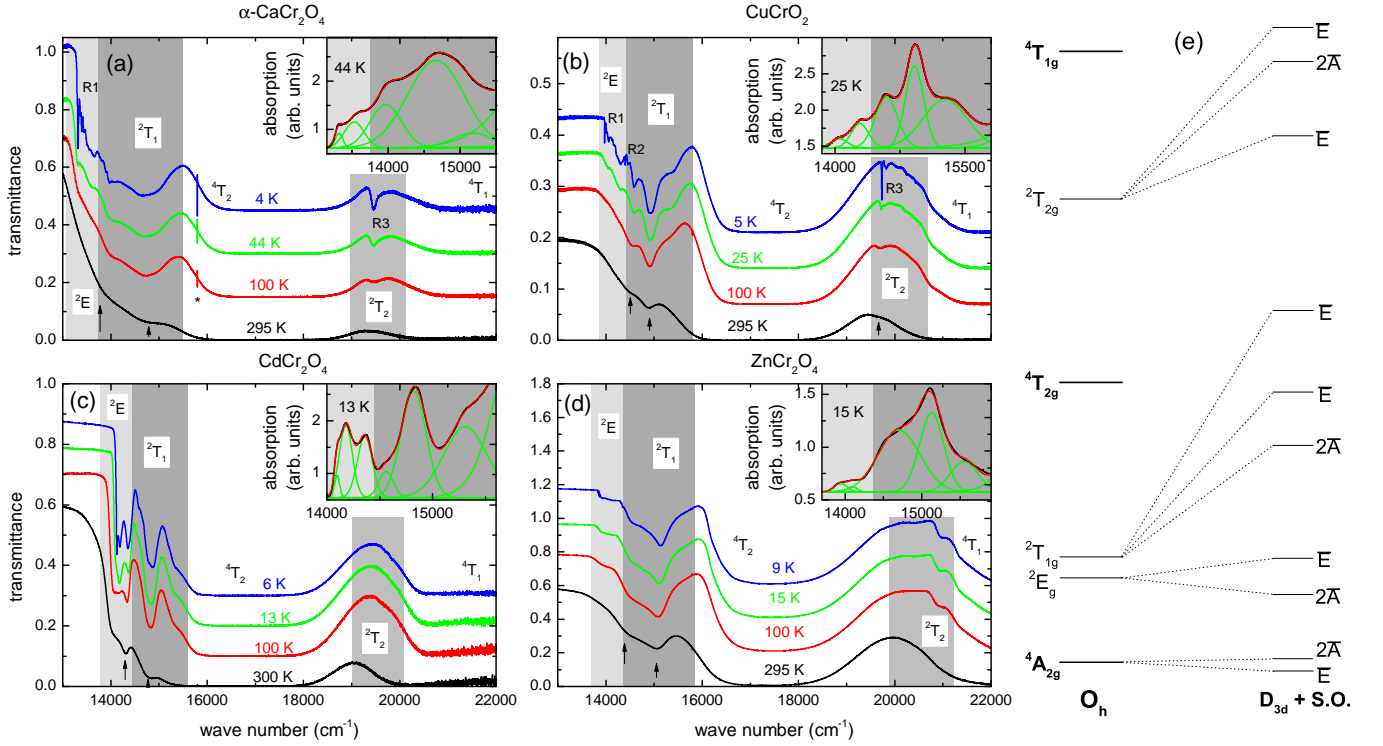


FIG. 2: (Color online) Transmission spectra for α - CaCr_2O_4 (a), CuCrO_2 (b), and ACr_2O_4 with $A=\text{Cd}$ (c), Zn (d) for several temperatures below and above the respective magnetic ordering temperatures. The lines are shifted for clarity. Up arrows mark the spin-forbidden transitions (shaded areas) already visible at room temperature and the asterisk in (a) an artifact due to the laser of the spectrometer. The insets in the top right corner of the frames are zooms into the lower energy absorption spectrum just above the magnetic ordering together with a fit to the data. Individual peaks are shown in green, while the sum is in red color. Frame (e) shows the transition scheme of a d^3 -ion in an octahedral crystal field O_h and the splitting due to the trigonal environment D_{3d} and spin-orbit coupling (S.O.) following Ref. [44].

detected. The magnetic susceptibility of our samples (not shown) is in good agreement with literature^{18,45}. A Curie-Weiss fit to the data between 200 and 400 K results in a Curie-Weiss temperature of 178 K, slightly lower than the values measured by Kimura *et al.*¹⁸ (211 K out of plane, 203 K in plane) from samples grown from Bi_2O_3 flux. Single crystals of α - CaCr_2O_4 were grown in a high temperature floating zone furnace as described elsewhere⁴⁶. The cleaved platelet is about 100 microns thick with a diameter of 3 mm. High-quality platelike single crystals of CdCr_2O_4 and ZnCr_2O_4 were prepared as described in Ref. [47] and polished to optical quality. The optical transmission was measured using a Bruker IFS 66v/S Fourier-transform spectrometer, which was equipped with a He-bath and a He-flow cryostat, in the frequency range 8500 - 25000 cm^{-1} and for temperatures from 5 - 500 K.

	α - CaCr_2O_4	CuCrO_2	CdCr_2O_4	ZnCr_2O_4
Mode 1	13317.7	14053.0	14096.0	13946.7
Mode 1*			14178.3	
Mode 2	13530.6	14286.4	14358.1	14099.5
Mode 3	13969.0	14593.3	14559.3	14702.1
Mode 4	14663.4	14916.5	14819.8	15126.7
Mode 5	15179.4	15268.9	15309.7	15549.2

TABLE I: Energies of the transitions between the t_{2g} levels for the different compounds in cm^{-1} obtained from a fit to the data just above the magnetic ordering temperature (see insets of Fig. 2).

III. EXPERIMENTAL RESULTS AND DISCUSSION

A. Crystal-field splitting of Cr^{3+}

In all systems investigated here the magnetic ions are Cr^{3+} ions with $3d^3$ electronic configuration surrounded by an octahedron of oxygen ions. In a perfect O_h symmetry, this would result in the usual splitting according

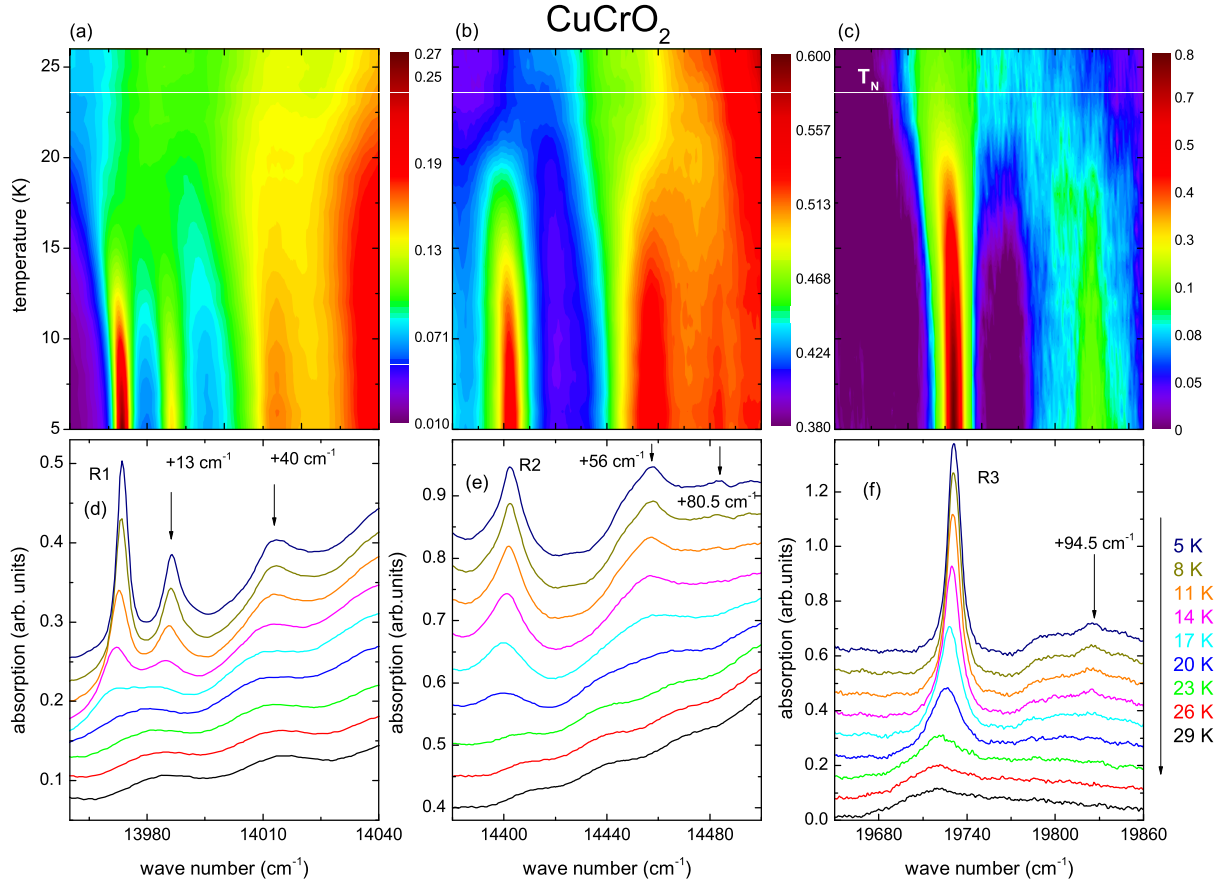


FIG. 3: (Color online) Color coded contour plot of the absorption as a function of temperature vs. wave number in the range of excitation R1 (a), R2 (b), and R3 (c). The transition temperature is marked as a white line. The lower part of the figure [(d)-(f)] shows absorption spectra in the same range as the respective frame on top for various temperatures. The curves are shifted for clarity by a constant value of 0.03 (d), 0.05 (e), and 0.075 (f). Sidebands are marked by arrows together with the energy difference to R1, R2 and R3, respectively.

to the Tanabe-Sugano diagram for d^3 ions⁴⁸ [see scheme in Fig. 2(e)]. However the symmetry for our compounds is rather trigonal D_{3d} , which leads to a further splitting of the excitations. Additionally, the modes are split by spin-orbit coupling. Wood *et al.*⁴⁴ investigated the crystal field excitations in ZnAl_2O_4 and MgAl_2O_4 doped with Cr ions both theoretically and experimentally. The Cr ions in these spinels are in a similar environment as in our case and the 2E_g mode splits by a few cm^{-1} and the 2T modes are split into three levels separated by a few 100 cm^{-1} . For ZnGa_2O_4 doped with Cr the splitting of the 2E_g multiplet increases to 40 cm^{-1} ⁴⁹, showing the sensitivity to the local symmetry. The spin allowed states can also evolve into several modes, but do not involve spin-flips and exciton-magnon transitions and will only shortly be discussed. The modes are very sensitive to a change in the crystal-field which can be seen as a linear dependence in the Tanabe-Sugano diagram. Vibrations of the octahedron, therefore, lead to a strong broadening of the lines. The scheme of excitations including the low symmetry and spin-orbit splitting of the spin-forbidden modes is shown in Fig. 2(e).

The parity selection rule which forbids transitions between the multiplet states in cubic symmetry can be released by a static low-symmetry crystal field with odd-parity or a corresponding odd lattice vibration inducing a low-symmetry field. As a result even-parity states will be mixed with odd-parity contributions and nonvanishing matrix elements of the electric dipole moment will occur.⁵⁰

In addition, no such matrix elements for transitions to multiplet states with different spin multiplicities (spin-forbidden crystal field transitions) exist, but this spin-selection rule ($\Delta S=0, 1$) can be released by spin-orbit coupling.

The NIR transmission spectra for all materials are shown in Fig. 2. The overall features are typical for Cr^{3+} ions in an octahedral crystal field like, for example, in ruby⁵¹. One can see two strong spin-allowed crystal-field absorptions in all compounds at about 17000 cm^{-1} and about 22000 cm^{-1} corresponding to ${}^4A_2 \rightarrow {}^4T_2$ and ${}^4A_2 \rightarrow {}^4T_1$ transitions, respectively, where one electron is excited from the t_{2g} to the e_g levels. These energies correspond to a cubic crystal field

splitting $10Dq \approx 17000 \text{ cm}^{-1}$ and a Racah parameter $B \approx 465 \text{ cm}^{-1}$. A splitting of the spin-allowed transitions due a crystal field lower than cubic or spin-orbit coupling can not be resolved.

The focus here is on the spin-forbidden transitions which are much weaker than the spin-allowed transitions. In cubic symmetry the spin-forbidden excitations $^4A_2 \rightarrow ^2E$, $^4A_2 \rightarrow ^2T_1$ and $^4A_2 \rightarrow ^2T_2$ are expected and already at room temperature weaker modes (indicated by arrows in Fig. 2) are visible. Towards lower temperature these absorption features become narrower and more pronounced and just above the magnetic ordering five distinct absorptions are identified in the region of the $^4A_2 \rightarrow ^2E$, $^4A_2 \rightarrow ^2T_1$ (see insets of Fig. 2). The energies of these are obtained by a fit and can be read off in Table I. Even for the lower symmetry of $\alpha\text{-CaCr}_2\text{O}_4$ the fit works well with 5 Gaussians in this region. In the case of CdCr_2O_4 an additional Gaussian was used to account for the shoulder at the low-energy flank of the 2E absorption region resulting in modes 1 and 1*.

B. Exciton-magnon transitions

Let us now turn to the spin-forbidden crystal field transitions within the t_2^3 states, in particular the $^4A_2 \rightarrow ^2E_2$ and the $^4A_2 \rightarrow ^2T_1$ transitions. In the transmission spectra very sharp excitonic absorption features accompanying these transitions are already visible in Fig. 2 [e.g. the ones labelled R1, R2, and R3 in Fig. 2(b)] at lowest temperatures. As proposed by Tanabe, Moriya, and Sugano such sidebands can occur when two ions on sites i and j are coupled antiferromagnetically and the electric-dipole moment of the incoming light couples an excited multiplet state of the ion at site i to the ground multiplet state of the ion at j .¹³ In this so-called electric-dipole induced exciton-magnon process with a total spin change $\Delta S = 0$, the spin-forbidden multiplet transitions can exhibit cold and hot magnon sidebands on the high- and low-energy side of the so-called zero-magnon line, corresponding to the annihilation and creation of a magnon, respectively.^{52–56} This zero-magnon line identifies the purely excitonic crystal-field transition. Depending on the complexity of the antiferromagnetic interactions and the spin configuration multi-magnon sidebands can be expected and have actually been observed in several compounds.^{57,58}

Moreover, the energy of the exciton-magnon sidebands with respect to the zero-magnon line should correspond to the magnon energy in regions of the Brillouin zone, where the dispersion is flat, i.e. where the magnon density of states peaks. Thus, optical spectroscopy can provide information on the magnon energies in the flat-regions of the Brillouin zone.⁵⁶ Since short-range correlations are sufficient to make these transitions allowed, the persistence of non-trivial spin correlations in the classical spin-liquid phase of frustrated magnets can be tracked by optical spectroscopy. In the following we will discuss the

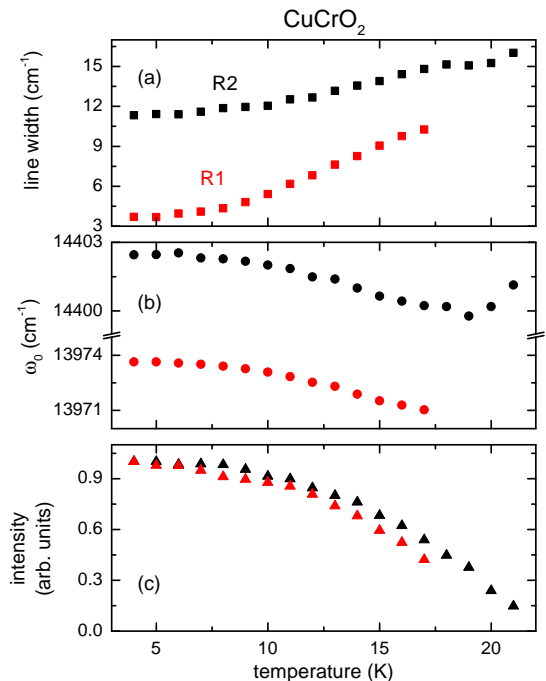


FIG. 4: (Color online) Fit parameters of exciton R1 (red) and R2 (black): (a) line width, (b) frequency and (c) intensity normalized to the value at 4 K.

observed exciton-magnon transitions separately for each of the investigated compounds.

1. CuCrO_2

In the magnetically ordered state pronounced fine structures, named R1, R2, and R3 in the following, appear at the onset of the $^4A_2 \rightarrow ^2E$, $^4A_2 \rightarrow ^2T_1$, and $^4A_2 \rightarrow ^4T_2$ excitations below the magnetic ordering temperature [see Fig. 3(a)-(c)]. As the two transition temperatures lie very close together, in the following only T_{N1} is used as T_N . Similar features have been reported below the respective Néel temperatures in a variety of Cr based magnets and assigned to purely excitonic lines and exciton-magnon sidebands^{12,42}. In the following we will restrict the discussion on these fine structures and their temperature dependences which are summarized in Fig. 3.

Zooming into the region of the fine structure close to the excitation R1 [Fig. 3(a) and (d)] three absorption features can be clearly seen at low temperatures. The first peak is assigned to a zero-magnon-line corresponding to a purely excitonic transition. The two sidebands with an energy difference of $+13 \text{ cm}^{-1}$ and $+40 \text{ cm}^{-1}$ with respect to the pure exciton line can be assigned to exciton-magnon sidebands by comparison to recent neutron scattering^{19,59,60} and high-field ESR studies⁶¹. The first sideband is very close in energy to the antiferromagnetic resonance (AFMR) observed in finite magnetic

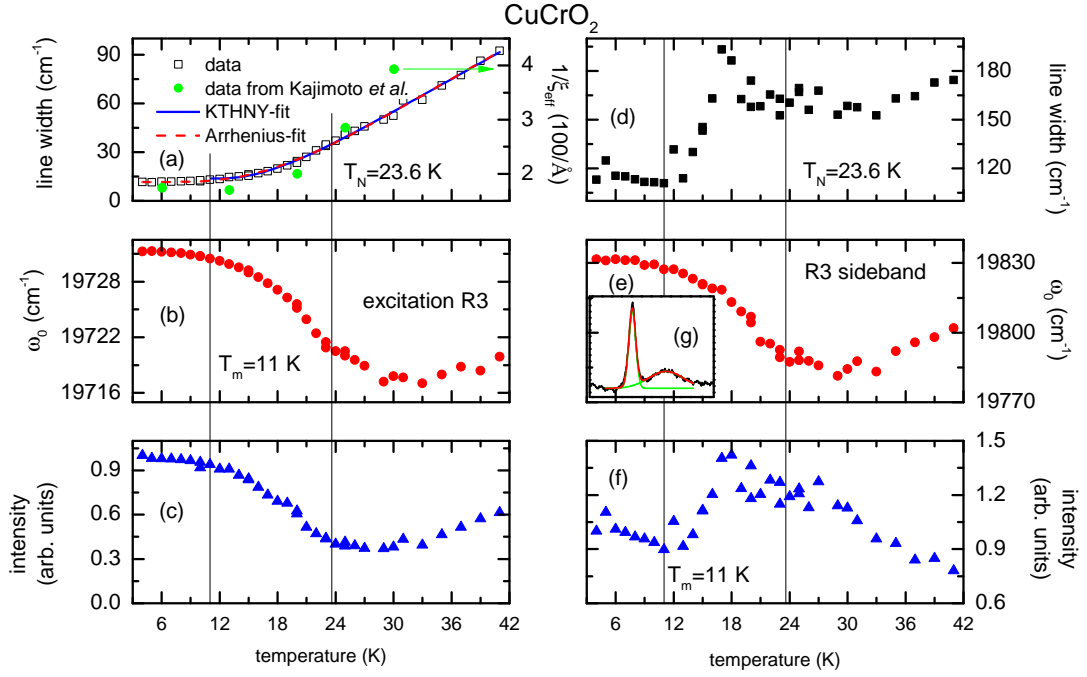


FIG. 5: (Color online) Fit parameters of exciton R3 (a) line width, (b) frequency and (c) intensity normalized to the value at 4 K and of the sideband of R3 (d)-(f), respectively. The red and blue line are fits to the line width data of excitation R3 with an Arrhenius model and the KTHNY-model, respectively (see text). The green circles in (a) are data for the inverse of the effective correlation length ξ_{eff} from Ref. [59]. In panel (g) an absorption spectrum at $T=18$ K is shown together with a fit using two Gaussians. The two individual peaks are in green and the sum of both in red color.

fields by Yamaguchi *et al.*⁶¹. The sideband energy of $+40$ cm^{-1} is in agreement with reported magnon bands around 5 meV with a bandwidth of about 1 meV in the vicinity of the zone boundary^{19,60}.

Similarly, the fine structure related to R2 also exhibits two sidebands, one peaked at a distance of $+56$ cm^{-1} from R2 with an additional shoulder and another weaker feature at a distance of $+80.5$ cm^{-1} [Fig. 3(b),(e)]. The latter energy can be associated with the predicted magnon energy at the zone-boundary arising due to an interlayer exchange coupling¹⁹, while the former can not be attributed to a single magnon branch, but corresponds to the energy range where overlapping magnon branches were reported.¹⁹

To analyze the temperature dependence of R1 and R2, we fitted the two lines with Gaussians after subtracting the background due to the spin-forbidden excitations by a polynomial fit to the data outside of the exciton range. The temperature dependence of the fit parameters can be seen in Fig. 4. Both, the position of the absorption maximum ω_0 [Fig. 5(b)] and the intensity [Fig. 4(c)] of the excitations R1 and R2, increase continuously towards lower temperatures reflecting the behavior of the sublattice magnetization in the magnetically ordered state. The line width (full width half maximum) of R1 nearly triples on rising temperature just before it vanishes while R2 shows a less pronounced broadening. This behavior is in agreement with the expected behavior for magnon

sidebands in an antiferromagnetic system and we can not resolve any features related to frustration or short-range order.

In contrast, the excitation R3 can be observed up to 45 K (about twice T_N) as a strongly broadened feature in the absorption. In Fig. 3(c) and (f) one can see the absorption spectrum around the excitation R3. It consists of a strong and sharp mode at 19730 cm^{-1} and a broad sideband feature at higher frequencies ($+94.5$ cm^{-1} from R3). We also fitted this range with two Gaussian lines for R3 and the broad sideband feature [see Fig. 5(g)]. The temperature dependence of the fit parameters are shown in Fig. 5. The magnetic ordering temperature shows up in the eigenfrequency ω_0 [Fig. 5(b)] as a kink, below which it increases to lower temperatures, reflecting the increase of an internal magnetic field. A similar behavior is observed for the intensity of R3 [Fig. 5(c)], but its line width [Fig. 5(a)] seems not to be influenced by the magnetic ordering at T_N . Previous investigations of the line width of the $^4A_2 \rightarrow ^2T_2$ absorption bands in the triangular lattice antiferromagnets LiCrO_2 , VX_2 ($X = \text{Cl, Br, I}$) and NaCrO_2 ^{11,12} have been interpreted in terms of the formation of Z_2 vortices,¹² i.e. the relaxation time of the magnon sidebands is determined by the density of Z_2 vortices for all these compounds.

This density of unbound Z_2 vortices should be inversely proportional to the correlation length of two vortices ξ given by¹

$$\xi = \xi_0 \exp \left[\frac{b}{(T/T_m - 1)^\alpha} \right]. \quad (1)$$

Here T_m corresponds to the melting temperature of the Z_2 vortices, i.e. the energy scale to overcome the bound-vortex state, and α is a characteristic exponent. Using the values of effective correlation length ξ_{eff} determined in neutron scattering measurements by Kajimoto *et al.*⁵⁹ [Fig. 5(a), green circles, right scale] we find a similar temperature dependence but a stronger increase than the line width of the excitation R3. Moreover, recent electron spin resonance (ESR) studies reported values for T_m and α for many compounds of the ACrO_2 series.^{9,10} The blue line in Fig. 5(a) shows a fit to our data using ξ^{-1} with the same values $T_m = 11$ K, $\alpha = 0.37$ as obtained in these ESR studies.¹⁰ In addition, we use the parameter $\Delta\omega_m$ for residual line width at T_m ($\Delta\omega_m = 13.8 \text{ cm}^{-1}$, $\xi_0 = 2.07 \times 10^{-4} \text{ cm}$, $b = 4.98$). The data is well described for $T > T_m$. Using an Arrhenius law

$$\Delta\omega = \Delta\omega_0 + B \exp \left[\frac{-E^*}{k_B T} \right], \quad (2)$$

a similarly good fit can be obtained with a characteristic temperature $E^* = 69$ K ($B = 431 \text{ cm}^{-1}$, $\Delta\omega_0 = 11.7 \text{ cm}^{-1}$, red dashed line). This value is comparable to the predicted energy cost of the breaking of two Z_2 vortices obtained by a Monte Carlo simulation $1.52JS^2 = 48$ K.⁶² Hence, we conclude that the temperature dependence of the lifetime of the transition R3 is in agreement with the predicted existence of Z_2 vortices in the triangular antiferromagnet CuCrO_2 . Interestingly, the broad sideband of R3 seems to exhibit a clear anomaly in line width and intensity at about the proposed melting transition $T_m = 11$ K [Fig. 5(d) and (f)]. This could indicate that the lifetime of the sideband excitation is strongly reduced, when the vortices unbind and enhance the scattering rate for magnons. On the other hand, the eigenfrequency [Fig. 5(e)] shows the same temperature dependence as the one of the zero-magnon line.

2. $\alpha\text{-CaCr}_2\text{O}_4$

Analogously to the case of CuCrO_2 we concentrate on the onset of the ${}^4A_2 \rightarrow {}^2E$ (R1) and on the ${}^4A_2 \rightarrow {}^2T_2$ (R3) bands. The corresponding absorption spectra are shown in Fig. 6(c) and (d) for several temperatures below and above the Néel temperature. The detailed temperature evolution is visualized in the color-coded plots in Fig. 6(a) and (b). In the case of the ${}^4A_2 \rightarrow {}^2E$ region one can clearly recognize the emergence of a fine structure, which we assign again to exciton-magnon transitions. The most intense absorption at 13315 cm^{-1} (named R1 as in the case of CuCrO_2) is identified as a purely excitonic line and several sidebands are visible both on the

low- and the high-energy side of R1. Hot magnon sidebands appear as shoulders at a distance of -16 cm^{-1} and -30 cm^{-1} to R1, while cold magnon sidebands are visible at a distance of $+51 \text{ cm}^{-1}$, $+78 \text{ cm}^{-1}$, and $+120 \text{ cm}^{-1}$.

A direct comparison with the magnetic excitation spectra determined by neutron scattering²⁵ reveals a number of low-lying spin wave modes at roughly the same energies. The excitation at -30 cm^{-1} corresponds to the interplane coupling of 3.5 meV . For all other modes direct correspondance can not be established, but soft magnetic modes are found between 2 meV (16 cm^{-1}) and 15 meV (120 cm^{-1}),²⁵ coinciding with the energies of the magnon sidebands.

The ${}^4A_2 \rightarrow {}^2T_2$ (R3) band only reveals the absorption R3 at 19450 cm^{-1} which broadens and seemingly disappears on approaching T_N from below, although a broad background contribution is still visible above the Néel temperature, which indicates the short-range order regime.

Following the same procedure as in the case of CuCrO_2 , we fit the absorption peaks R1 and R3 using Gaussian line shapes. The fit parameters are shown in Fig. 7. The excitation R1 can be followed up to 41 K. The eigenfrequency shows the typical increase to lower temperatures and, as expected, the line width increases strongly when approaching the magnetic ordering temperature from below. Notably, the intensity exhibits a broad maximum at around 30 K marked by an arrow in the figure, before it becomes nearly constant towards lowest temperatures. An anomaly below the Néel temperature at about 24 K has also been found by ESR measurement, recently,⁶³ confirming the possible existence of a further energy scale in the system. The excitation R3 can be tracked as a very broad feature up to 70 K. The eigenfrequency is almost constant below T_N , but increases for $T > T_N$. The line width is slightly increasing on approaching T_N from below and shows a similar increase as the eigenfrequency above T_N . The intensity is decreasing with increasing temperature, showing the strongest decrease in the vicinity of T_N . Although an anomaly below the Néel temperature may exist in this compound, it seems that exciton-magnon excitations are more dominated by the antiferromagnetic phase transition than by features associated with the existence of Z_2 vortices.

3. CdCr_2O_4 and ZnCr_2O_4

The absorption spectra in the region of the spin-forbidden ${}^4A_2 \rightarrow {}^2E$ and ${}^4A_2 \rightarrow {}^2T_1$ crystal-field excitations of CdCr_2O_4 and ZnCr_2O_4 are shown for several temperatures in Fig. 8(a) and (b), respectively. The temperature evolution of the spectra in ZnCr_2O_4 is rather continuous and the broad absorption peaks sharpen with decreasing temperature as expected in case of phonon-assisted transitions. In addition, the smooth onsets of the transition bands sharpen up and below the magneto-

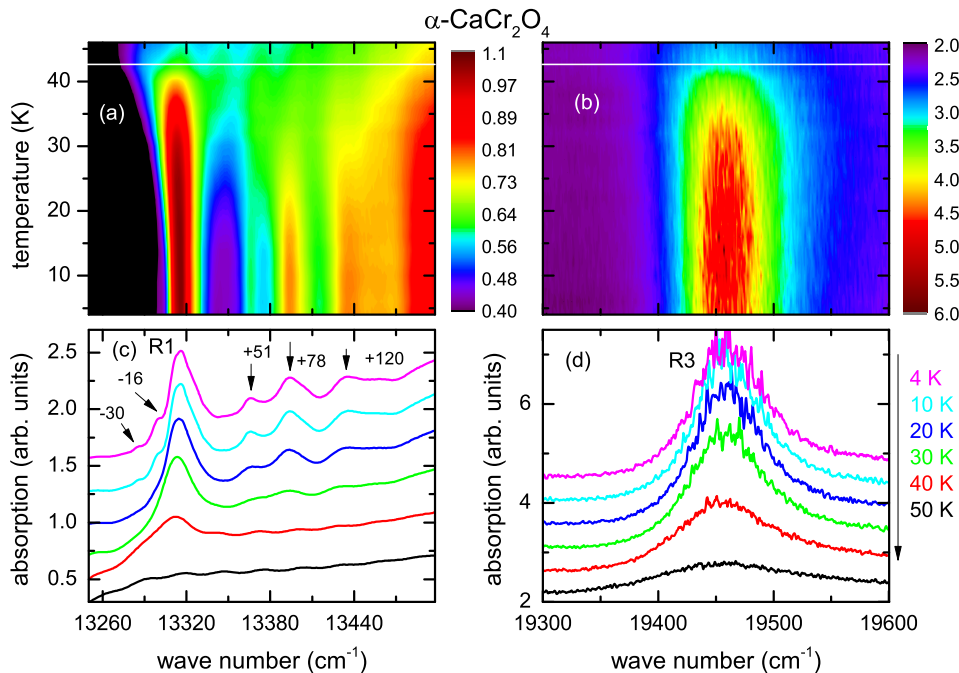


FIG. 6: (Color online) Color coded contour plot of the absorption as a function of temperature vs. wave number in the range of excitation 2E (a) and 2T_2 (b). T_N is shown as a white line. The lower part of the figure (c), (d) shows absorption spectra in the same range as the respective frame on top for various temperatures. The curves are shifted for clarity by a constant value of 0.3 (c) and 0.5 (d). Sidebands are marked by arrows together with the energy difference to the excitonic line.

structural transition the onset is edge-like and exhibits a very weak fine structure. The lowest-temperature spectrum is shown in an enlarged scale in Fig. 9(b). This group of narrow excitonic lines (further zoomed in the gray inset) has previously been observed by Szymczak *et al.* and attributed to the Davydov splitting of the two lowest single-ion levels of the 2E state.⁶⁴ Interestingly, very similar spectra have also been obtained and analyzed for exchange-coupled Cr^{3+} pairs in non-magnetic ZnGa_2O_4 .⁶⁵ These authors identified the observed fine structure in terms of exciton-magnon processes and vibronic sidebands. Remarkably, the obtained values for the exchange coupling constants in dilute systems are in very good agreement with the ones obtained for ZnCr_2O_4 itself.^{34,66} Above the magnetic ordering temperature this fine structure is smeared out.

The rather broad absorption band at 15150 cm^{-1} associated with ${}^4A_{2g} \rightarrow {}^2T_1$ has been suggested to stem from an exciton-magnon-phonon (EMP) transition,⁶⁴ which has recently been reported to be suppressed in fields above 400 T.⁴³ We traced its temperature evolution to temperatures above the CW temperature as shown in Fig. 8(b) and still observe a broad maximum at the highest measured temperatures. This suggests that this excitation might not be governed by spin correlations, but rather correspond to a more conventional CF excitation.

In the case of CdCr_2O_4 one can clearly see the emergence of two new modes M_0 and M_3 related to the ${}^4A_2 \rightarrow {}^2E$ transition. In the magnetically ordered state the onset becomes very sharp and is governed by the

sharp narrow mode M_0 at 14125 cm^{-1} which we assign to the purely excitonic transition. In an enlarged scale [see Fig. 9(a)] shoulders are visible in the spectrum at a distance $\pm 17(2)\text{ cm}^{-1}$ from M_0 . These sidebands can be attributed to a hot (M_{-1}) and cold magnon (M_1) sideband. The magnetic excitation spectrum of CdCr_2O_4 has been studied by neutron scattering and spin wave excitations with energies $m_a = 0.65\text{ meV}$ (5.2 cm^{-1}), $m_b = 2.3\text{ meV}$ (18.6 cm^{-1}) and $m_c = 4.7\text{ meV}$ (37.9 cm^{-1}) were reported at the wave vector $(1, 0.915, 0)$ associated with the zone center of the incommensurate spin structure.⁶⁷ We identify $M_{\pm 1}$ within the experimental uncertainty with the magnon branch m_b , which reportedly is only slightly dispersive.⁶⁷ In a high-field ESR study up to ten magnetic excitation modes have been observed and attributed to higher-harmonics of helical spin-resonance modes.⁶⁸ A recent analysis confirmed this idea and identified the magnetic excitation spectrum as due to highly dispersive helimagnons.⁶³ The excitation M_3 occurs at a distance of $+61.7\text{ cm}^{-1}$ from the purely excitonic line M_0 and can be understood in terms of a cold exciton-three-magnon transition, where all three magnon branches are involved as $(m_a + m_b + m_c) = 61.7\text{ cm}^{-1}$.

Notably, both the one-magnon sidebands $M_{\pm 1}$ and the excitonic mode M_0 can not be detected above the magnetic ordering temperature. However, the excitation M_3 remains clearly visible with increasing temperature and seems to persist up to the Curie-Weiss temperature of about 70 K, where the absorption spectrum seems to become plateau-like. This suggests that short-range helical

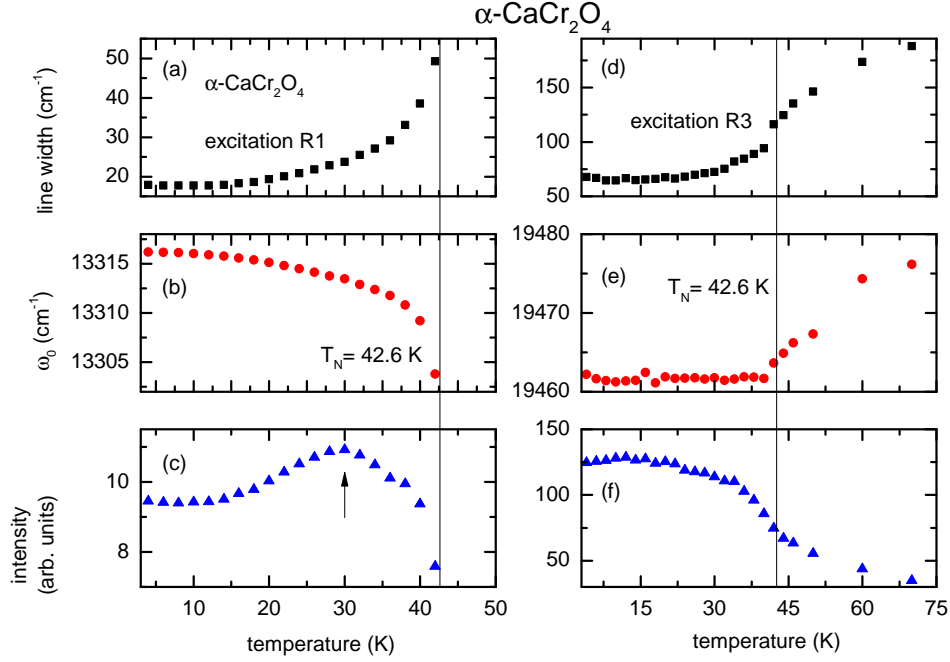


FIG. 7: (Color online) Fit parameters of exciton R1 (left side) and R3 (right side) (a),(d) line width, (b),(e) frequency and (c),(f) intensity, respectively. The arrow in (c) marks a maximum at 30 K.

spin correlations may already exist throughout the classical spin-liquid regime $T_N < T \leq \Theta_{CW}$.

A direct comparison of the two low-temperature absorption spectra of CdCr_2O_4 and ZnCr_2O_4 is presented in Fig. 9(c), where the spectra are plotted vs. wave number scaled to the respective onset wave number ν_0 of the exciton lines. In case of CdCr_2O_4 ν_0 was defined as the purely excitonic line M_0 and in case of ZnCr_2O_4 the first peak of the fine structure at 13835 cm^{-1} was used. The absorption values are scaled in a way that the curves coincide at the maximum of the absorption peak visible at $\nu/\nu_0 = 1.05$ for CdCr_2O_4 . In this scaling, even the low-energy flanks of the two curves coincide and the peak maximum in CdCr_2O_4 corresponds to a clear shoulder in ZnCr_2O_4 . Moreover, the EMP feature in ZnCr_2O_4 seems to correspond to a shoulder in the spectrum of CdCr_2O_4 [see shaded areas in Fig. 9(c)]. This shoulder is directly followed by the first spin-allowed crystal-field excitation in CdCr_2O_4 . We propose that the occurrence of similar features in both compounds and their persistence to the highest studied temperatures (exceeding the respective Curie-Weiss transitions) again favors a structural origin of these excitations. Therefore, the reported suppression of the EMP peak above 400 T might be interpreted as a magnetic-field induced structural change.⁴³ This scaling further suggests that the $^4A_2 \rightarrow ^2E$ and $^4A_2 \rightarrow ^2T_1$ regions are behaving differently in terms of relative intensities for the two compounds, i.e. the $^4A_2 \rightarrow ^2E$ and $^4A_2 \rightarrow ^2T_1$ regions appear to be of comparable intensity in CdCr_2O_4 , while the $^4A_2 \rightarrow ^2T_1$ region seems to have much higher intensity in ZnCr_2O_4 . This might be

related to the different structural distortions in the two systems in the magnetically ordered state. There is still a debate with respect to the exact symmetry of the two systems,^{47,69,70} but a clear difference is that in ZnCr_2O_4 the lattice contracts and in CdCr_2O_4 it elongates along the c -axis. This will certainly influence the transition probabilities and the intensities of the CF transitions.

IV. SUMMARY

In summary, we observed exciton-magnon transitions in the triangular-lattice antiferromagnets CuCrO_2 and $\alpha\text{-CaCr}_2\text{O}_4$ and in the spinel CdCr_2O_4 . Some of the magnon sidebands in these three systems can be directly compared to the spin-wave dispersions reported by neutron scattering studies and reflect the respective complex magnetic structures:

(i) In CuCrO_2 three sets of fine structures have been observed to emerge with lowering temperature. The first four of the related sideband energies of $+13$, $+40$, $+56$, $+81$, and $+95 \text{ cm}^{-1}$ are in agreement with magnon energies observed by antiferromagnetic resonance and neutron scattering experiments, while for the last one no direct correspondence could be obtained. However, this magnon sideband at $+95 \text{ cm}^{-1}$ from the purely excitonic feature R3 at 19730 cm^{-1} exhibits an anomaly in the temperature dependence of its line width and intensity at about 11 K. This temperature is in agreement with a reported estimate of a binding-unbinding transition of Z_2 vortices. Moreover, the temperature dependence of

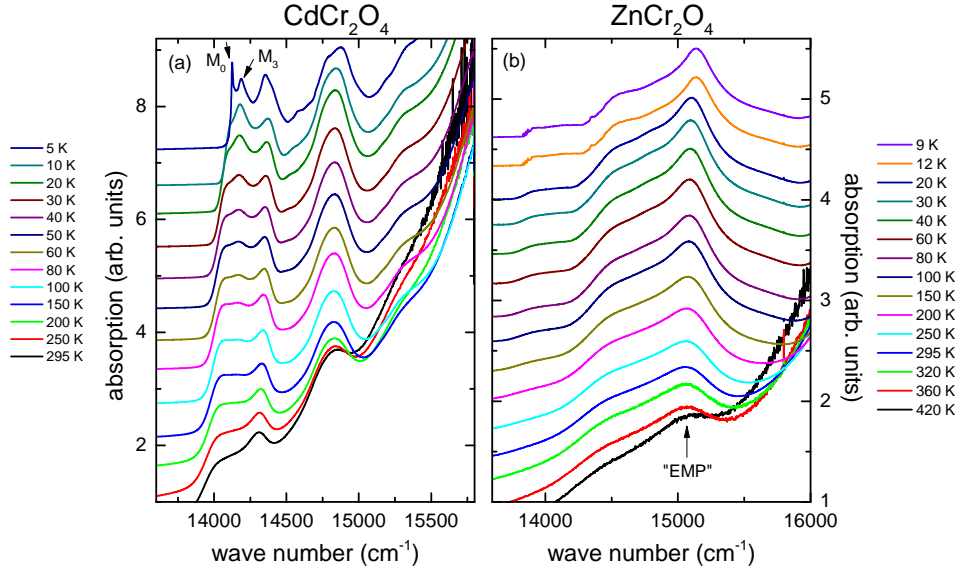


FIG. 8: (Color online) Absorption spectra of CdCr_2O_4 (a) and ZnCr_2O_4 (b) for various temperatures in the energy region of the excitations within the t_{2g} levels. The spectra are shifted for clarity by 0.55 (CdCr_2O_4) and 0.29 (ZnCr_2O_4)

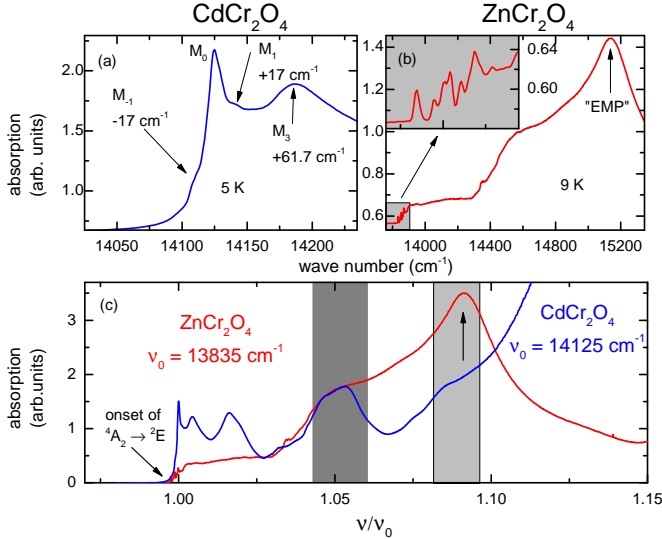


FIG. 9: (Color online) Zoom into the lower energy part of the absorption spectrum of CdCr_2O_4 (a) and ZnCr_2O_4 (b). For the latter the grey part is shown in an inset in an extended view. (c) shows a scaled version of the spectra. For details of the scaling see text.

the line width of the purely excitonic line R3 can be understood by assuming that the magnon lifetime is determined by the density of topologically protected Z_2 vortices.

(ii) In $\alpha\text{-CaCr}_2\text{O}_4$, several magnon sidebands at -16 , -30 , $+51$, $+78$, and $+120 \text{ cm}^{-1}$ have been observed. The interplane coupling of 3.5 meV corresponds well to

the sideband at -30 cm^{-1} . The other modes can not be unambiguously assigned on the basis of the currently available neutron scattering data, but several low-lying magnon modes have been reported in a similar energy range.²⁵

(iii) In CdCr_2O_4 magnon sidebands at ± 17 and $+61.7 \text{ cm}^{-1}$ have been observed at lowest temperatures. The first magnon energy corresponds to a single magnon observed by neutron scattering and the second sideband can be understood as a three-magnon sideband, where all three spin-wave excitations observed by neutron scattering at 5.2 , 18.6 , and 37.9 cm^{-1} are participating. Moreover, the three-magnon sideband remains visible up to the Curie-Weiss temperature of about 70 K pointing to the formation of short-range helical spin correlations throughout the classical spin-liquid regime.

However, in the spinel ZnCr_2O_4 only a weak fine structure has been observed in agreement with a previous report. The temperature dependence of an absorption (EMP) reportedly associated with the magnetic structure and suppressed in very high-magnetic fields suggests a primarily structural origin of this excitation in contrast to previous interpretations.

Acknowledgments

We want to thank M.V. Eremin, N. Perkins, H.-A. Krug von Nidda, M. Hemmida, and O. Tchernyshyov for fruitful discussions. We acknowledge partial support by the Deutsche Forschungsgemeinschaft via TRR 80 (Augsburg-Munich) and project DE 1762/2-1.

- ¹ H. Kawamura, A. Yamamoto, and T. Okubo, J. Phys. Soc. Jpn. **79**, 023701 (2010).
- ² B. Bernu, P. Lecheminant, C. Lhuillier, and L. Pierre, Phys. Rev. B **50**, 10048 (1994).
- ³ H. Kawamura and S. Miyashita, J. Phys. Soc. Jpn. **53**, 9 (1984).
- ⁴ S. Seki, Y. Onose, and Y. Tokura, Phys. Rev. Lett. **101**, 067204 (2008).
- ⁵ Y. Ajiro, H. Kikuchi, S. I. Sugiyama, T. Nakashima, S. Shamoto, N. Nakayama, M. Kiyama, N. Yamamoto, and Y. Oka, J. Phys. Soc. Jpn. **57**, 2268 (1988).
- ⁶ A. Olariu, P. Mendels, F. Bert, B. G. Ueland, P. Schiffer, R. F. Berger, and R. J. Cava, Phys. Rev. Lett. **97**, 167203 (2006).
- ⁷ D. Hsieh, D. Qian, R. F. Berger, R. J. Cava, J. W. Lynn, Q. Huang, and M. Z. Hasan, Physica B **403**, 1341 (2008).
- ⁸ D. Hsieh, D. Qian, R. F. Berger, R. J. Cava, J. W. Lynn, Q. Huang, and M. Z. Hasan, J. Phys. Chem. Solids **69**, 3174 (2008).
- ⁹ M. Hemmida, H. A. K. von Nidda, N. Buttgen, A. Loidl, L. K. Alexander, R. Nath, A. V. Mahajan, R. F. Berger, R. J. Cava, Y. Singh, et al., Phys. Rev. B **80**, 054406 (2009).
- ¹⁰ M. Hemmida, H. A. K. von Nidda, and A. Loidl, J. Phys. Soc. Jpn. **80** (2011).
- ¹¹ P. R. Elliston, F. Habbal, N. Saleh, G. E. Watson, K. W. Blazey, and H. Rohrer, J. Phys. Chem. Solids **36**, 877 (1975).
- ¹² N. Kojima, K. Ito, I. Mogi, M. Takeda, G. Kido, Y. Nakagawa, M. Sakai, N. Kuroda, and Y. Nishina, J. Phys. Soc. Jpn. **62**, 4137 (1993).
- ¹³ Y. Tanabe, T. Moriya, and S. Sugano, Phys. Rev. Lett. **15**, 1023 (1965).
- ¹⁴ H. Kadowaki, H. Kikuchi, and Y. Ajiro, J. Phys. Condens. Matter **2**, 4485 (1990).
- ¹⁵ M. Poienar, F. Damay, C. Martin, V. Hardy, A. Maignan, and G. Andre, Phys. Rev. B **79**, 014412 (2009).
- ¹⁶ K. Kimura, T. Otani, H. Nakamura, Y. Wakabayashi, and T. Kimura, J. Phys. Soc. Jpn. **78**, 113710 (2009).
- ¹⁷ M. Soda, K. Kimura, T. Kimura, M. Matsuura, and K. Hirota, J. Phys. Soc. Jpn. **78**, 124703 (2009).
- ¹⁸ K. Kimura, H. Nakamura, K. Ohgushi, and T. Kimura, Phys. Rev. B **78**, 140401 (2008).
- ¹⁹ M. Frontzek, J. T. Haraldsen, A. Podlesnyak, M. Matsuda, A. D. Christianson, R. S. Fishman, A. S. Sefat, Y. Qiu, J. R. D. Copley, S. Barilo, et al., Phys. Rev. B **84**, 094448 (2011).
- ²⁰ H. Pausch and H. K. Müllerbuschbaum, Z. Anorg. Allg. Chem. **405**, 113 (1974).
- ²¹ L. C. Chapon, P. Manuel, F. Damay, P. Toledano, V. Hardy, and C. Martin, Phys. Rev. B **83**, 024409 (2011).
- ²² S. Toth, B. Lake, S. A. J. Kimber, O. Pieper, M. Reehuis, A. T. M. N. Islam, O. Zaharko, C. Ritter, A. H. Hill, H. Ryll, et al., Phys. Rev. B **84**, 054452 (2011).
- ²³ K. Singh, C. Simon, and P. Toledano, Phys. Rev. B **84**, 064129 (2011).
- ²⁴ L. Zhao, T.-W. Lan, K.-J. Wang, C.-H. Chien, T.-L. Hung, J.-Y. Luo, W.-H. Chao, C.-C. Chang, Y.-Y. Chen, M.-K. Wu, et al., Phys. Rev. B **86**, 064408 (2012).
- ²⁵ S. Toth, B. Lake, K. Hradil, T. Guidi, K. C. Rule, M. B. Stone, and A. T. M. N. Islam, Phys. Rev. Lett. **109**, 127203 (2012).
- ²⁶ S. E. Dutton, E. Climent-Pascual, P. W. Stephens, J. P. Hodges, A. Huq, C. L. Broholm, and R. J. Cava, J. Phys. Condens. Matter **23**, 246005 (2011).
- ²⁷ G.-W. Chern, R. Moessner, and O. Tchernyshyov, Phys. Rev. B **78**, 144418 (2008).
- ²⁸ Y. Yamashita and K. Ueda, Phys. Rev. Lett. **85**, 4960 (2000).
- ²⁹ O. Tchernyshyov, R. Moessner, and S. L. Sondhi, Phys. Rev. Lett. **88**, 067203 (2002).
- ³⁰ A. B. Sushkov, O. Tchernyshyov, W. Ratcliff II, S. W. Cheong, and H. D. Drew, Phys. Rev. Lett. **94**, 137202 (2005).
- ³¹ C. J. Fennie and K. M. Rabe, Phys. Rev. Lett. **96**, 205505 (2006).
- ³² R. ValdésAguilar, A. B. Sushkov, Y. J. Choi, S.-W. Cheong, and H. D. Drew, Phys. Rev. B **77**, 092412 (2008).
- ³³ T. Rudolf, C. Kant, F. Mayr, M. Schmidt, V. Tsurkan, J. Deisenhofer, and A. Loidl, Euro. Phys. J. B **68**, 153 (2009).
- ³⁴ C. Kant, J. Deisenhofer, T. Rudolf, F. Mayr, F. Schrettle, A. Loidl, V. Gnezdilov, D. Wulferding, P. Lemmens, and V. Tsurkan, Phys. Rev. B **80**, 214417 (2009).
- ³⁵ C. Kant, M. Schmidt, Z. Wang, F. Mayr, V. Tsurkan, J. Deisenhofer, and A. Loidl, Phys. Rev. Lett. **108**, 177203 (2012).
- ³⁶ M. T. Rovers, P. P. Kyriakou, H. A. Dabkowska, G. M. Luke, M. I. Larkin, and A. T. Savici, Phys. Rev. B **66**, 174434 (2002).
- ³⁷ S.-H. Lee, C. Broholm, T. H. Kim, W. Ratcliff II, and S.-W. Cheong, Phys. Rev. Lett. **84**, 3718 (2000).
- ³⁸ T. Rudolf, C. Kant, F. Mayr, J. Hemberger, V. Tsurkan, and A. Loidl, Phys. Rev. B **75**, 052410 (2007).
- ³⁹ S.-H. Lee, C. Broholm, W. Ratcliff, G. Gasparovic, Q. Huang, T. H. Kim, and S.-W. Cheong, Nature **418**, 856 (2002).
- ⁴⁰ J.-H. Chung, M. Matsuda, S.-H. Lee, K. Kakurai, H. Ueda, T. J. Sato, H. Takagi, K.-P. Hong, and S. Park, Phys. Rev. Lett. **95**, 247204 (2005).
- ⁴¹ K. Tomiyasu, T. Inami, and N. Ikeda, Phys. Rev. B **70**, 184411 (2004).
- ⁴² H. Szymczak, W. Wardzynski, and A. Pajaczkowska, J. Magn. Magn. Mater. **15-18, Part 2**, 841 (1980), ISSN 0304-8853.
- ⁴³ A. Miyata, H. Ueda, Y. Ueda, H. Sawabe, and S. Takeyama, Phys. Rev. Lett. **107**, 207203 (2011).
- ⁴⁴ D. L. Wood, G. F. Imbusch, R. M. Macfarlane, P. Kisliuk, and D. M. Larkin, J. Chem. Phys. **48**, 5255 (1968).
- ⁴⁵ T. Okuda, N. Jufuku, S. Hidaka, and N. Terada, Phys. Rev. B **72**, 144403 (2005).
- ⁴⁶ A. Islam, S. Toth, and B. Lake, to be published.
- ⁴⁷ C. Kant, F. Mayr, T. Rudolf, M. Schmidt, F. Schrettle, J. Deisenhofer, and A. Loidl, Euro. Phys. J. Special Topics **180**, 43 (2010).
- ⁴⁸ S. Sugano, Y. Tanabe, and H. Kamimura, *Multiplets of Transition-Metal Ions in Crystals*, Pure and applied physics (Academic Press, 1970).
- ⁴⁹ H. M. Kahan and R. M. Macfarlane, J. Chem. Phys. **54**, 5197 (1971).
- ⁵⁰ S. Sugano, T. Zukito, and H. Kamimura, *Multiplets of Transition-Metal Ions in Crystals*, vol. 33 of PURE AND

- APPLIED PHYSICS* (Academic Press, New York, London, 1970).
- ⁵¹ D. L. Wood, J. Ferguson, K. Knox, and J. F. Dillon, *J. Chem. Phys.* **39**, 890 (1963).
 - ⁵² K. I. Gondaira and Y. Tanabe, *J. Phys. Soc. Jpn.* **21**, 1527 (1966).
 - ⁵³ Y. Tanabe and K.-I. Gondaira, *J. Phys. Soc. Jpn.* **22**, 573 (1967).
 - ⁵⁴ K. Shinagawa and Y. Tanabe, *J. Phys. Soc. Jpn.* **30**, 1280 (1971).
 - ⁵⁵ T. Fujiwara, W. Gebhardt, Y. Tanabe, and K. Petanide, *J. Phys. Soc. Jpn.* **33**, 39 (1972).
 - ⁵⁶ V. V. Eremenko, Y. G. Litvinenko, and E. V. Matyushkin, *Phys. Rep.* **132**, 55 (1986).
 - ⁵⁷ S. Sugano and N. Kojima, eds., *Magneto-Optics* (Springer, 2000).
 - ⁵⁸ J. Deisenhofer, I. Leonov, M. V. Eremkin, C. Kant, P. Ghigna, F. Mayr, V. V. Iglamov, V. I. Anisimov, and D. van der Marel, *Phys. Rev. Lett.* **101**, 157406 (2008).
 - ⁵⁹ R. Kajimoto, K. Nakajima, S. Ohira-Kawamura, Y. Inamura, K. Kakurai, M. Arai, T. Hokazono, S. Oozono, and T. Okuda, *J. Phys. Soc. Jpn.* **79**, 123705 (2010).
 - ⁶⁰ M. Poienar, F. Damay, C. Martin, J. Robert, and S. Petit, *Phys. Rev. B* **81**, 104411 (2010).
 - ⁶¹ H. Yamaguchi, S. Otomo, S. Kimura, M. Hagiwara, K. Kimura, T. Kimura, and K. Kindo, *J. Low Temp. Phys.* **159**, 130 (2010).
 - ⁶² T. Okubo and H. Kawamura, *J. Phys. Soc. Jpn.* **79**, 084706 (2010).
 - ⁶³ E. Choi, G.-W. Chern, and N. B. Perkins, arXiv:1205.4225v1 (unpublished).
 - ⁶⁴ H. Szymczak, W. Wardzynski, and P. A., *J. Magn. Magn. Matter.* **15-18**, 841 (1980).
 - ⁶⁵ G. G. P. van Gorkom, J. C. M. Henning, and R. P. van Staple, *Phys. Rev. B* **8**, 955 (1973).
 - ⁶⁶ C. Kant, J. Deisenhofer, V. Tsurkan, and A. Loidl, *J. Phys.: Conf. Ser.* **200**, 032032 (2010).
 - ⁶⁷ J. H. Chung, M. Matsuda, S. H. Lee, K. Kakurai, H. Ueda, T. J. Sato, H. Takagi, K. P. Hong, and S. Park, *Phys. Rev. Lett.* **95**, 247204 (2005).
 - ⁶⁸ S. Kimura, M. Hagiwara, H. Ueda, Y. Narumi, K. Kindo, H. Yashiro, T. Kashiwagi, and H. Takagi, *Phys. Rev. Lett.* **97**, 257202 (2006).
 - ⁶⁹ G.-W. Chern, C. J. Fennie, and O. Tchernyshyov, *Phys. Rev. B* **74**, 060405(R) (2006).
 - ⁷⁰ S. Ji, S.-H. Lee, C. Broholm, T. Y. Koo, W. Ratcliff, S.-W. Cheong, and P. Zschack, *Phys. Rev. Lett.* **103**, 037201 (2009).